Photoemission satellites and electronic structure of Fe_2O_3

A. Fujimori, M. Saeki, and N. Kimizuka
National Institute for Research in Inorganic Materials, 1-1Namiki, Sakura-mura, Niihari-gun, Ibaraki 305, Japan

M. Taniguchi and S. Suga
Synchrotron Radiation Laboratory, Institute for Solid State Physics, The University of Tokyo, Midori-cho, Tanashi, Tokyo 188, Japan

(Received 30 June 1986)

The electronic structure of α-Fe_2O_3 with the high-spin d^5 ground-state configuration has been studied by ultraviolet photoemission spectroscopy with use of synchrotron radiation as well as by x-ray photoemission and Auger-electron spectroscopy. The results are interpreted in terms of the configuration-interaction theory based on a FeO_6-cluster model. The main lines of the valence-band photoemission spectra are identified with Fe $3d^5$—ligand-hole final states produced by ligand-to-$3d$ charge-transfer screening of $3d$ holes ($3d^4$ states), whereas the satellite at higher binding energies is assigned to unscreened (or poorly screened) $3d^4$ final states. The Fe $3d$ versus O $2p$ partial density of states and symmetry characteristics of $3d$-derived peaks are found to be quite different from assignments based on ligand-field theory or band theory. These results indicate that Fe_2O_3 cannot be considered as a Mott-Hubbard insulator in its original sense but is classified as a charge-transfer-type insulator according to a theory of Zaanen, Sawatzky, and Allen. A possibility is suggested that the lowest unoccupied state is not Fe $3d$—like but is the bottom of the Fe $4s$ band. The large exchange energy of the high-spin $3d^5$ configuration is shown to greatly stabilize the localized $3d$ states relative to the itinerant state.

I. INTRODUCTION

Recent theoretical[1] and experimental[2,3] studies on the photoemission spectra of NiO have given basically new insight into the electronic structure of this compound. It has been found that hybridization between the localized, strongly correlated Ni $3d$ levels and the bandlike O $2p$ levels is essential and that charge transfer betwen these levels screens d electrons and holes created in photoemission, Auger-electron emission, and inverse photoemission [i.e., bremsstrahlung isochromat spectroscopy (BIS)] processes.[1-3] By considering configuration interactions (CI) including charge transfer between the $3d$ and ligand orbitals, the main lines of the valence-band photoemission spectrum, which are located near the valence-band maximum and had long been interpreted as d^7 final-state multiplet lines within the framework of the ligand-field (LF) theory,[4] are found to be $d^8\underline{L}$ final states ($\underline{L}$ is the ligand hole) resulting from $L \rightarrow d$ charge transfer screening of d holes (d^7 states), whereas the high binding energy satellite is found to be unscreened (or poorly screened) d^7 final states.[1] Namely, the spectrum consisting of the main and satellite features result from an $L \rightarrow d$ shake-down process. This finding combined with the fact that the lowest unoccupied states are Ni $3d^9$ (Ref. 3) has led to a conclusion that the band gap is not a Mott-Hubbard (d-d) type in its original sense,[5] where the magnitude is determined by the on-site d-d Coulomb correlation energy U. Instead, the gap is interpreted as an $L \rightarrow d$ charge-transfer type determined by the $L \rightarrow d$ charge-transfer energy or the electronegativity difference between the $3d$ and ligand orbitals rather than only by U.[3] In fact, this picture was supported by a subsequent photoemission-BIS experiment[6,7] and a theoretical calculation[7] on NiS, in which the band gap between occupied $d^8\underline{L}$ and empty d^9 states disappears owing to the low electronegativity of S compared with O.

Based on this idea, Zaanen, Sawatzky, and Allen[8] have developed a general theory for metal-insulator transitions in $3d$ transition-metal compounds, and have classified the compounds into several groups including the charge-transfer and Mott-Hubbard regimes. According to the theory, the system enters the Mott-Hubbard regime with decreasing electronegativity of the transition-metal atom or with increasing electronegativity of the ligand atom. In this regime the lower (smaller) binding energy band (referred to as the main band) is d^{n-1}-like rather than $d^n\underline{L}$, that is, the satellite at a higher (larger) binding energy results from shake-up transitions, and the band gap is of the d-d type with a magnitude of $\sim U$. In this context, Zaanen *et al.* have postulated that Ti and V compounds are in the Mott-Hubbard regime, while Cu, Ni, and Co compounds are in the charge-transfer regime. In order to test the validity of this metal-insulator transition mechanism and settle a boundary between the two regimes in real materials, systematic spectroscopic studies on transition-metal compounds are required. Such quantitative studies have so far been limited to Ni compounds including NiO,[1,7] $NiCl_2$,[1] and NiS.[7]

In this paper, we report experimental and theoretical results on α-Fe_2O_3 (hematite), which is a so-called Mott insulator. It is also expected that the results will provide basic data to interpret photoemission spectra of more complicated Fe-O systems such as valence-fluctuating

Fe_3O_4,[9] whose electronic structure has long been a matter of controversy,[10] and oxidized Fe surfaces.[11] Fe_2O_3 is an antiferromagnetic (weakly ferromagnetic above 260 K) insulator like NiO and crystallizes in the α-corundum (α-Al_2O_3) structure where an Fe atom is octahedrally coordinated by six O atoms. The ground-state configuration of Fe is high-spin d^5, i.e., ^6S or $^6A_{1g}$ in the cubic representation. According to the LF theory[12] the Fe $3d$–derived photoemission spectrum is quite simple: Two multiplet lines, $^5T_{2g}$ and ^5E_g, with an intensity ratio of 3:2 are separated by the crystal-field splitting Δ_{CF}. In Fig. 1 an assignment based on the LF theory for another representative high-spin d^5 system MnO is shown.[4] The valence-band spectrum of Fe_2O_3 shows the same characteristic features as MnO, namely the three-peak structure in the main band (within ~ 7 eV of the valence-band maximum) and a satellite at higher binding energies, which have been interpreted in the same manner.[13] The band theory also predicts only two d peaks, t_{2g} and e_g bands, separated by Δ_{CF} with the same intensity ratio.[14] In the following sections, however, we will show that the main band is due to $d^5\underline{L}$ final states which are screened via $L \rightarrow d$ charge transfer while the satellite is due to unscreened d^4 final states. Consequently, it is concluded that Fe_2O_3 is not a Mott-Hubbard insulator but a charge-transfer insulator like NiO. It is interesting to compare the present results with the band theory, as the band theory appears to explain the photoemission spectra apart from the satellite,[14,15] and predicts their changes with crystal structure and magnetic ordering.[16]

In Sec. II experimental details are given. Results of x-ray and ultraviolet photoemission spectroscopy (XPS and UPS), Auger electron spectroscopy, and resonant photoemission in the Fe $3p \rightarrow 3d$ core excitation region are presented and interpreted on the basis of the CI picture in Sec. III. The photoemission experiments in a wide photon energy range and, in particular, the resonant behavior of the spectra allowed us to obtain information on the Fe $3d$ and O $2p$ partial density of states (DOS), namely, the distribution of d^4 and $d^5\underline{L}$ final-state characters. Section IV describes the CI calculation of the valence-band photoemission spectrum using the FeO_6 cluster model. Several physical implications are discussed in Sec. V.

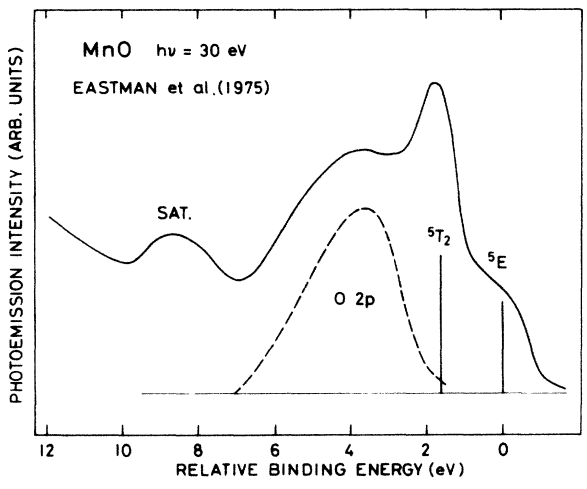

FIG. 1. Valence-band UPS spectrum of MnO which has the same $3d$-electron configuration as Fe_2O_3 with its interpretation based on the ligand-field theory, after Ref. 4. (The intensity ratio of the $^5T_{2g}$ and ^5E_g in Ref. 4, was erroneous and has been corrected.) The satellite was explained as a result of ligand-to-d shake-up transitions.

II. EXPERIMENTAL

XPS, UPS, and x-ray excited Auger electron spectra were recorded with a spectrometer equipped with an unmonochromatized Mg $K\alpha$ radiation source ($h\nu = 1253.6$ eV) and a He resonance lamp ($h\nu = 21.2$ and 40.8 eV), where photoelectrons were collected with a PHI 15-255 double-pass cylindrical mirror analyzer. The base pressure of the spectrometer was $\sim 1 \times 10^{-10}$ Torr.

UPS spectra using synchrotron radiation ($35 \leq h\nu \leq 120$ eV) were taken at the Synchrotron Radiation Laboratory of The University of Tokyo. A Rowland-mount monochromator and a cylindrical mirror analyzer of the same type as that for XPS were used. The total resolution was ~ 0.5 eV for photon energies $h\nu \sim 50$ eV. Measurements were performed under a vacuum of $\sim 1 \times 10^{-10}$ Torr. Spectra were taken in the constant pass energy mode and were subsequently corrected for the analyzer transmission. All spectra were normalized to the photon flux in order to obtain constant initial state (CIS) spectra. Photoabsorption in the Fe $3p \rightarrow 3d$ excitation region was recorded by measuring the total photoelectron yield with an ammeter connected to the sample.

The samples were a sintered pellet and a single crystal grown by the chemical vapor transport method using HCl as a transport agent. The sintered sample had been reduced in air at ~ 1390 °C for 17 h and made electrically conductive in order to avoid charging effects during photoemission measurements. That treatment had resulted in $\sim 10\%$ of Fe atoms in the Fe_3O_4 phase, but this amount of the second phase is expectedly too small to give noticeable features characteristic of Fe_3O_4. In fact, spectra taken on both samples were found virtually identical. UPS spectra presented in this paper are of the sintered sample. As charging effects for XPS and x-ray excited Auger electron spectra were only to shift the whole spectra uniformly to higher binding energies (by ~ 7 eV) without any noticeable broadening, we present XPS and Auger electron spectra taken on the single-crystal sample with a corrected energy scale. All binding and kinetic energies have been referenced to the Fermi level (E_F) of the spectrometer.

The samples were scraped *in situ* with a diamond file, and the cleanliness was checked with XPS by the absence of both the C $1s$ peak and the high binding energy component of the O $1s$ peak which may arise from adsorbed water or carbon oxides. The present XPS spectra are in good agreement with those reported previously,[13,17] where clean sample surfaces were prepared by grinding in an inert-gas atmosphere or heating in an ultrahigh vacuum. A UPS spectrum for $h\nu = 21.2$ eV is somewhat different from the previous one[13] probably because of much less surface contamination in the present experiment.

III. RESULTS

A. Valence-band photoemission

Figure 2 shows photoemission spectra in the valence-band region for a wide range of photon energies. The spectra may be divided into the main band (1—10 eV) and satellite (10—17 eV) regions. The main band consists of three features at ~2.5, ~5, and ~7 eV. According to the LF theory, the former two peaks are assigned to d^4 multiplet and the third one to the anion p band as in the case of Mn^{2+} compounds such as MnO[4] (Fig. 1) and Mn halides.[18,19] However, it turns out that this assignment is not consistent with the photon energy dependence of the atomic-orbital cross sections as described below.

It is well known that the O $2p$ cross section steeply increases toward lower photon energies while the Fe $3d$ emission becomes more dominant for higher photon energies. In particular, below $h\nu \sim 40$ eV, the Fe $3d$ cross section decreases with decreasing photon energies and becomes much smaller than that of O $2p$ at $h\nu \sim 20$ eV.[20] One notices that in contrast to such different photon energy dependences of the Fe $3d$ and O $2p$ cross sections the three-peak structure of the main band remains relatively intense with rather unchanged line shape for the whole photon energy range. Thus we consider that all these features have mixed Fe $3d$—O $2p$ character. Further, from the spectra for $h\nu < 100$ eV (particularly from the 21.2-eV spectrum corrected for the secondary electron background shown by a solid curve in Fig. 2), O $2p$ emission can be located at ~4 eV rather than at ~7 eV as in the previous assignment.[13] The XPS spectrum of isostructural Al_2O_3 shows two O $2p$ peaks separated by ~4 eV, where the shallower one is assigned to nonbonding O $2p$ states and the deeper to Al $3sp$—O $2p$ bonding states.[21] We assign the structure at ~4 eV to nonbonding O $2p$ states which are enhanced relative to the bonding states for low photon energies, $h\nu \sim 20$ eV. Fe $4sp$—O $2p$ bonding states may then be located around ~8 eV. As for the satellite (10—17 eV), its intensity relative to the main band increases monotonously with increasing photon energies. This result indicates that the satellite is more Fe $3d$—like than the main band.

The above results can be consistently interpreted within the CI picture with consideration of the hybridization of d^4 and $d^5\underline{L}$ configurations in the photoemission final states[1]. The satellite is assigned to d^4 final states, whereas the main band is to $d^5\underline{L}$ final states which result from $L \rightarrow d$ charge-transfer screening of d holes (d^4 states). Thus the Fe $3d$—derived emission is not a simple d^4 multiplet, namely one $^5T_{2g}$ and one ^5E_g line, but of more complicated multiplet of mixed d^4 and $d^5\underline{L}$ configurations as will be calculated in Sec. IV.

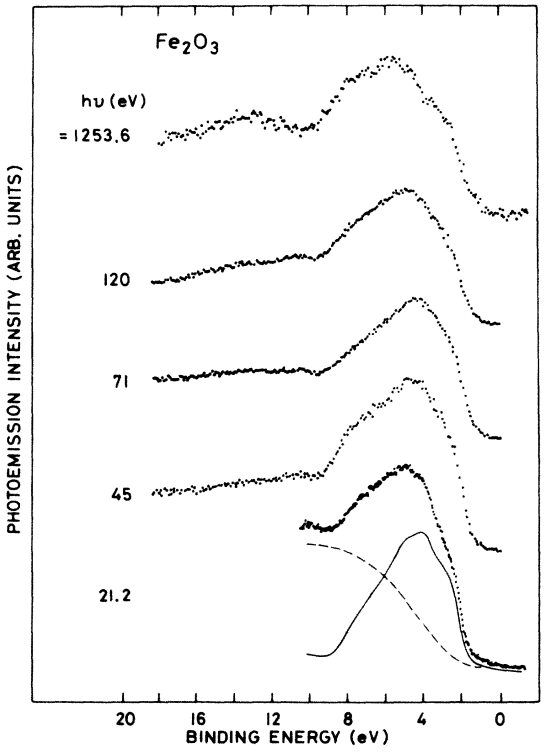

FIG. 2. Valence-band photoemission spectra of Fe_2O_3 for various photon energies. The solid curve for $h\nu = 21.2$ eV is a result after subtracting an integral background (dashed curve).

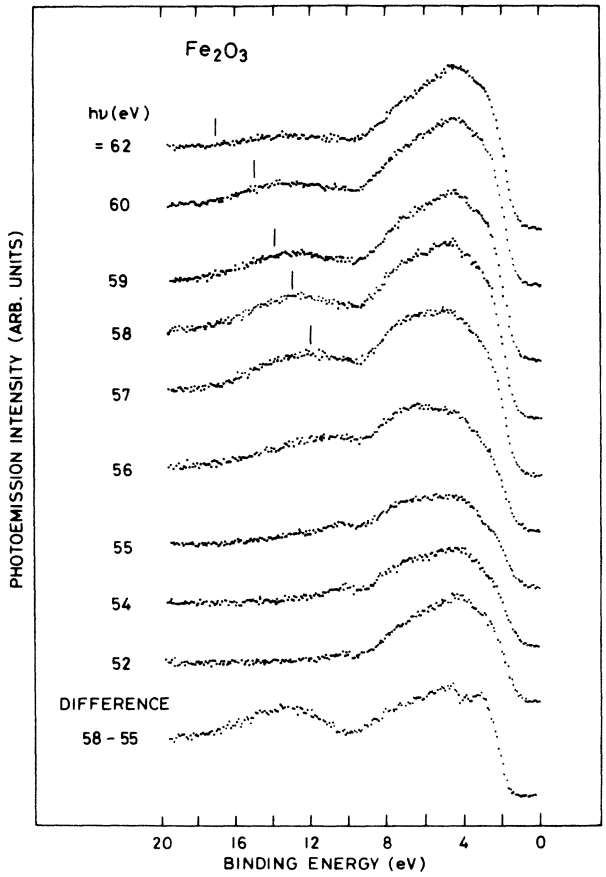

FIG. 3. Valence-band UPS spectra of Fe_2O_3 for photon energies in the $3p \rightarrow 3d$ excitation region. A constant kinetic energy of 45 eV is marked by vertical bars for photon energies above the Fe $3p$ threshold, where $M_{2,3}M_{4,5}M_{4,5}$ Auger emission would be expected. The bottom panel shows a difference curve (vertical scale multiplied by 1.3) between on- ($h\nu = 58$ eV) and off-resonance ($h\nu = 55$ eV) spectra highlighting the Fe $3d$—derived emission.

B. Fe 3p core absorption and resonant photoemission

For photon energies in the Fe 3p-core excitation region, the Fe 3d—derived photoemission intensity is enhanced through a resonant photoemission process, i.e., interference between direct photoemission ($3d^n \rightarrow 3d^{n-1} + \varepsilon_l$) and Auger electron emission ($3p^5 3d^{n+1} \rightarrow 3p^6 3d^{n-1} + \varepsilon_l$) following the $3p \rightarrow 3d$ core excitation.[22] As has been demonstrated for Ni^{2+} and Cu^{2+} compounds,[1,23] resonant photoemission can be used to distinguish between d^{n-1} and $d^n\underline{L}$ final states, because d^{n-1} final states usually show a Fano-type resonance peak near the $3p \rightarrow 3d$ threshold while for $d^n\underline{L}$ final states an antiresonance dip on the lower photon energy side of the Fano peak is accentuated.

Figure 3 shows valence-band photoemission spectra taken for photon energies near the 3p core-level binding energy with a small photon energy interval, and Fig. 4 shows CIS spectra and the total photoelectron yield spectrum. The CIS curves of the three features in the main band (particularly those for $E_B = 2.3$ and 4.5 eV) are rather of the anti-resonance-type while the satellite (the CIS for $E_B = 12.7$ eV) clearly shows a resonance peak. The Fe 3d—derived nature of the 7-eV feature which has not been considered in the LF theory is again evident from the CIS spectrum and the difference spectrum between on- and off-resonance spectra as shown on the bottom of Fig. 3. Above the Fe 3p core threshold, $M_{2,3}M_{4,5}M_{4,5}$ Auger emission at a constant kinetic energy is expected as indicated by vertical bars in Fig. 3. However, the Auger emission is too weak to be identified in contrast to the case of Fe_3O_4,[9] similarly to other insulating Fe compounds such as $FeCl_2$ and $FeBr_2$.[19]

In Fig. 4, the absorption profile consists of a dominant peak at $h\nu = 58$ eV corresponding to ^6P atomic term of the $3p^5 3d^6$ configuration and a subsidiary peak at $h\nu = 53.5$ eV corresponding to ^6F and ^6D terms.[24] Besides, a broad hump is seen on the higher-energy side of the main features at $h\nu \simeq 60$—70 eV. Similar high-energy features which cannot be explained by the $3p^5 3d^{n+1}$ multiplet have been observed for the 3p absorption spectra of various transition-metal halides.[25] These features may arise from transitions into metal 4s states, or could be attributed to a $3p^5 3d^7\underline{L}$ satellite as opposed to the main $3p^5 3d^6$ features as has been identified for NiO and Ni halides.[26] If this assignment is correct, the $3d^5\underline{L}$-like photoemission final states will be more enhanced than the $3d^4$ final states at $h\nu \simeq 60$—70 eV, since the $3p^5 3d^7\underline{L}$ states mostly decay via an Auger process $3p^5 3d^7\underline{L} \rightarrow 3p^6 3d^5\underline{L} + \varepsilon_l$. In fact, the CIS spectra for $E_B = 2.3$ and 4.5 eV show a weak, broad hump in this photon energy range, while that for $E_B = 12.7$ eV does not.

C. Core-level photoemission

In Fig. 5 XPS spectra in the Fe 2p, 3p, and 3s core-level regions are shown. Every core peak is accompanied

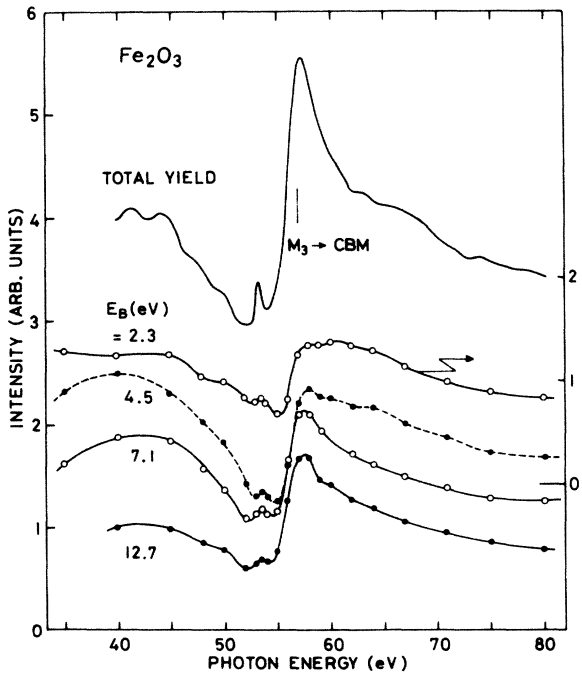

FIG. 4. Constant initial state (CIS) spectra and the total photoelectron yield of Fe_2O_3. The threshold energy for the Fe $3p_{3/2}$ core excitation obtained from the core-level binding energy (56 eV) and the band gap (2.7 eV, after Ref. 31) is shown by a vertical bar. The vertical scale for the CIS spectrum of $E_B = 2.3$ eV is shown on the right, while that for the other CIS spectra and the total photoelectron yield spectra is shown on the left.

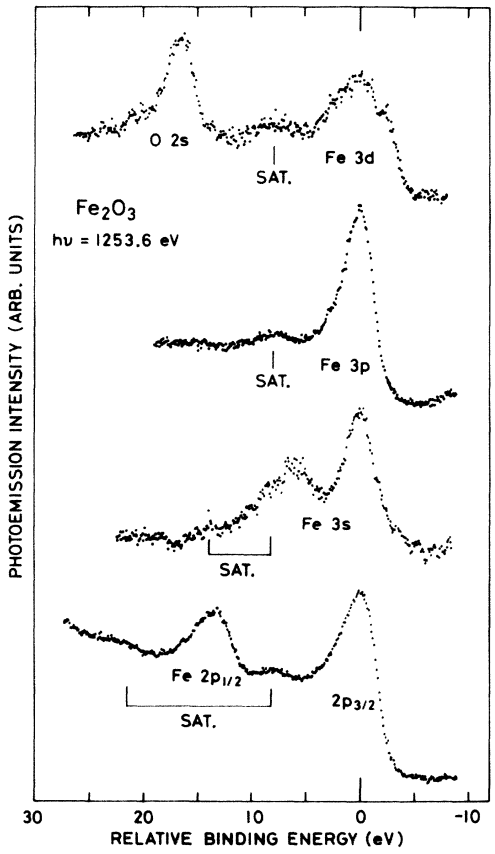

FIG. 5. Valence-band and core-level XPS spectra of Fe_2O_3. For each main peak a satellite appears at a higher binding energy of about 8 eV.

by a satellite feature on the high binding energy side as in the valence-band spectrum. (The Fe $3s$ peak is split into ^7S and ^5S components separated by 6 eV through exchange interaction with the magnetic $3d^5$ shell. The $j=\frac{1}{2}$ component of the Fe $3p$ level does not give a well-defined peak but is spread over a wide energy range of ~ 30 eV probably due to intraatomic correlation.[27]) As no similar satellites are found for O levels, these satellites are certainly associated with excitations or screening involving Fe $3d$ orbitals at the core-hole site. The fact that the position and the intensity of the satellite relative to the main line are similar for all the core levels and the valence band would suggest the localized nature of the $3d$-electron emission. Also the similarity between the core and the valence levels suggests that the core-level main lines are $L\rightarrow d$ screened $\underline{c}3d^6\underline{L}$ final states, where $\underline{c}$ denotes the core hole, whereas the satellites are poorly screened $\underline{c}3d^5$ states. This assignment is different from the traditional one which assumes $L\rightarrow d$ shake-up transitions in the core-hole final states[28] but is consistent with a recent assignment by Veal *et al.*,[29] who have concluded on the basis of local-density calculations that for various $3d$ transition-metal compounds the main and satellite core-level peaks are ascribed to local ($3d$) and nonlocal (mainly $4sp$) screening channels, respectively.

D. Auger-electron spectroscopy

The Fe $L_3M_{4,5}M_{4,5}$ ($2p$-$3d$-$3d$) and $M_{2,3}M_{4,5}M_{4,5}$ ($3p$-$3d$-$3d$) Auger spectra are shown in Figs. 6 and 7, respectively. Each Auger emission consists of a broad single peak. The broadness of the spectrum would be due to the multiplet structure of final-state two-hole configurations (d^3, $L\rightarrow d$ screened $d^4\underline{L}$ or $d^5\underline{L}^2$).

Since the kinetic energies of Auger electrons are lowered by the Coulomb correlation energy between the two final-state holes, one might expect to obtain the on-site d-d correlation energy U from the Auger results. However, we note that the initial-state hole and the final-state holes in the Auger process are not unscreened d holes but are d holes screened by $L\rightarrow d$ charge-transfer processes if the above assignment for the valence-band and core-level satellite structures is considered. In fact, the traditional assignment ignoring the $L\rightarrow d$ screening leads to an unreasonably small U. If we assign the core-level and valence-band main peaks to unscreened $\underline{c}3d^5$ and $3d^4$ states, respectively, and the Auger peak to $3d^3$, the Auger-electron kinetic energy $E^A_{\rm kin}$ is given by

$$E^A_{\rm kin}=E_B(\underline{c}3d^5)-2E_B(3d^4)-U\ . \tag{1}$$

By using the Auger-electron kinetic energies and the core-level binding energies listed in Table I, we obtain from Eq. (1) $U\simeq 1$ eV which is comparable to the $3d$ bandwidth[30] and is smaller than the band gap of Fe_2O_3, 2.0–2.7 eV, deduced from the electrical conductivity in the intrinsic conduction region.[31] On the other hand, if we take into account $L\rightarrow d$ screening effects, the Auger-electron kinetic energy is, by neglecting energy shifts due to hybridization between different configurations, given by

$$E^A_{\rm kin}\simeq E_B(\underline{c}3d^6\underline{L})-2E_B(\underline{L})-U_{\rm eff} \tag{2a}$$

if the Auger final state is assigned to $d^5\underline{L}^2$, or

$$E^A_{\rm kin}\simeq E_B(\underline{c}3d^6\underline{L})-E_B(\underline{L})-E_B(3d^4)-U_{\rm eff} \tag{2b}$$

if it is assigned to $d^4\underline{L}$. Using $E_B(\underline{L})\simeq 4.5$ eV and $E_B(3d^4)\simeq 13$ eV (the binding energies of the main and satellite peaks of the valence band, respectively), the former case [Eq. (2a)] gives $U_{\rm eff}\simeq 1$ eV between two ligand holes (or two holes in the $d^6\underline{L}$ band), while the latter case [Eq. (2b)] gives $U_{\rm eff}\simeq -7$ eV between a $3d$ and a ligand

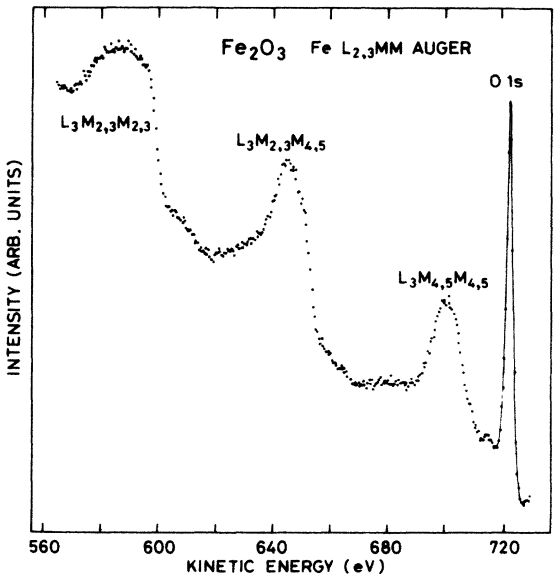

FIG. 6. Fe $L_{2,3}MM$ Auger spectrum of Fe_2O_3 excited with Mg $K\alpha$ radiation. Each of the three L_3MM peaks is accompanied by an L_2MM emission at ~ 14 eV higher kinetic energy, which has been considerably weakened relative to the L_3MM emission due to the $L_2L_3M_{4,5}$ Coster-Kronig process. Also each Auger peak has a weak, broad feature at ~ 20 eV lower kinetic energy which may be assigned to a poorly screened satellite.

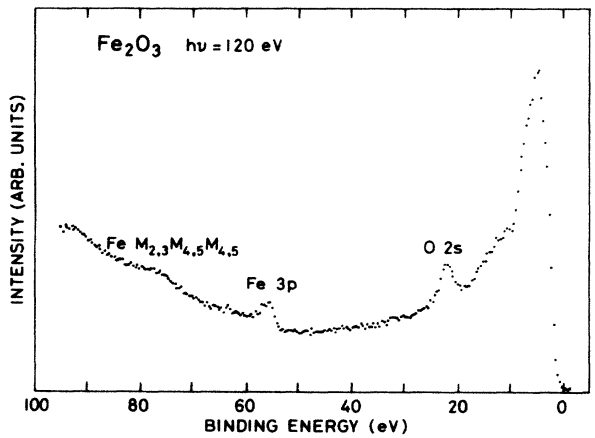

FIG. 7. Photoemission spectrum of Fe_2O_3 taken for $h\nu=120$ eV for a wide binding energy range showing Fe $M_{2,3}M_{4,5}M_{4,5}$ Auger emission.

TABLE I. Binding energies of core-level main peaks and kinetic energies of Auger electron peaks relative to E_F (in eV; the accuracy is ±0.2 eV unless otherwise stated).

Fe $2p_{3/2}$	$2p_{1/2}$	$3s$[a]	$3p$	$L_3M_{4,5}M_{4,5}$	$M_{2,3}M_{4,5}M_{4,5}$	O $1s$
711.2	724.6	94.2	56.0	700.9±0.5	45±1	530.2

[a]The binding energy of the ^7S component. The ^7S-^5S splitting is 6.0±0.2 eV.

hole. Since U_{eff} in either case is expected to be a small positive number of the order of 1 eV or less, we conclude that the former assignment, $d^5\underline{L}^2$, is a proper one. This conclusion appears reasonable in that two holes on a Fe site are screened by transfer of two electrons from the ligands to the Fe atom while a single hole is screened by transfer of one electron. Thus the charge-transfer screening mechanism is found important not only for photoemission but also for Auger electron spectroscopy, and consequently U cannot be generally obtained directly from Auger electron spectroscopy. Coulomb correlation energies so far obtained from Auger-electron spectroscopy for some $3d$ transition-metal oxides[9,32] would thus correspond to U_{eff} rather than U.

IV. CONFIGURATION-INTERACTION CLUSTER CALCULATION

In order to substantiate the above spectral assignment and to obtain more quantitative information on the electronic structure of α-Fe_2O_3, we have performed a CI calculation on the FeO_6^{9-} cluster model following the same procedure as applied to NiO and $NiCl_2$.[1] The cluster simulates the local environment of a single Fe ion in the corundum lattice, where two trigonally distorted FeO_6 octahedrons share an O_3 face. The charge of the cluster is derived from the formal charges of the Fe^{3+} and O^{2-} ions. As the trigonal distortion of the cluster would have only minor effects on the photoemission spectra, it is ignored in the present calculation and we will use the notation for the cubic symmetry O_h.

In Fig. 8, energy levels in the CI cluster theory are schematically shown for the ground state as well as for the photoemission and BIS final states. The energies of these final states relative to the ground state are measured with the emitted or incident electron at the Fermi level, E_F. That is, the energies are referenced to E_F which is located $\sim$1.7 eV above the valence-band maximum. The covalency of the ground state is represented by a mixture of $d^6\underline{L}$ configuration into the high-spin d^5 ($t_2^3e^2$) configuration with ^6S or $^6A_{1g}$ symmetry of the purely ionic Fe^{3+}. The ground-state wave function is given by

$$\Psi_g(^6A_1)=a_0\,|\,t_2^3e^2\,^6A_1\rangle+a_1\,|\,t_2^3e^3\underline{L}_\sigma\,^6A_1\rangle+a_2\,|\,t_2^4e^2\underline{L}_\pi\,^6A_1\rangle\ , \tag{3}$$

where $\underline{L}_\sigma$ and $\underline{L}_\pi$ denote molecular orbitals with E_g and T_{2g} symmetry, respectively, consisting of O $2p$ atomic orbitals in the cluster. The Hamiltonian for the ground state is of the form[33]

$$H=\begin{bmatrix} E_5+\Delta(^6A_1) & \sqrt{2}v_\sigma & \sqrt{3}v_\pi \\ \sqrt{2}v_\sigma & E_5+\delta E_A+\Delta(^5E) & 0 \\ \sqrt{3}v_\pi & 0 & E_5+\delta E_A+\Delta(^5T_2) \end{bmatrix}, \tag{4}$$

where $\Delta(^{2S+1}\Gamma)$ is the energy of the $^{2S+1}\Gamma$ term relative to the center of gravity of that configuration[34] and is given in terms of Racah parameters B and C.[35] Here, $\delta E_A\equiv E(d^5\rightarrow d^6\underline{L})\sim\varepsilon_d-\varepsilon_L+U$ is the energy required to transfer an electron from the ligand to Fe $3d$ orbitals in the ground state. ($\varepsilon_d\equiv\varepsilon_d^0+4U$ is the energy required to add an electron to the d^4 configuration, where ε_d^0 is the $3d$-orbital energy for $U\rightarrow 0$.) v_σ and v_π are defined in terms of Fe $3d$–O $2p$ transfer integrals as $v_\sigma=-\sqrt{3}(pd\sigma)$ and $v_\pi=-2(pd\pi)$. The final state for d-electron emission has either ^5E_g or $^5T_{2g}$ symmetry and is of the form

$$\Psi_f(^{2S+1}\Gamma)=b_{f0}\,|\,d^{4\,2S+1}\Gamma\rangle+\sum_i b_{fi}\,|\,d^5\underline{L}^{\,2S+1}\Gamma\rangle_i+\sum_j b_{fj}\,|\,d^6\underline{L}^{2\,2S+1}\Gamma\rangle_j\ . \tag{5}$$

The explicit form of the basis functions and the Hamiltonian matrix elements for the final states as well as for the ground states are given in Table II. Transition-matrix elements for d-electron emission are listed in Table III.

In calculating the valence-band photoemission spectra, energy differences between different configurations, i.e., δE_A in the initial state as well as $\delta E_B\equiv E(d^4\rightarrow d^5\underline{L})\sim\varepsilon_d-\varepsilon_L$ and $\delta E_C\equiv E(d^5\underline{L}\rightarrow d^6\underline{L}^2)\sim\varepsilon_d-\varepsilon_L+U$ in the final states (see Fig. 8) were treated as adjustable parameters. These energies and consequently U are substantially reduced from those estimated based on free-ion energy levels because of the polarization of the solid-state environment including charge transfer between O $2p$ and Fe $4sp$ orbitals, which is not explicitly included in the present formalism. The transfer integrals $(pd\sigma)$ and $(pd\pi)$ were also allowed to vary with a constraint $(pd\pi)/(pd\sigma)=-0.5$. B and C parameters have been tak-

TABLE II. Basis functions and Hamiltonian matrix elements for the FeO_6^{9-} and FeO_6^{8-} clusters representing, respectively, the ground state and photoemission final states of Fe_2O_3. $K=E_5+(15+\frac{5}{9})B-(7+\frac{7}{9})C$; $L=E_5+\delta E_A+(23+\frac{1}{3})B-(11+\frac{2}{3})C$; $\Delta=\varepsilon(e_g)-\varepsilon(t_{2g})$; $\delta=\sqrt{2}[(pp\pi)-(pp\sigma)]$ (set to be zero in the present work); $P=E_4+(9+\frac{1}{3})B+(4+\frac{2}{3})C$; $Q=E_4+\delta E_B+(15+\frac{5}{9})B+(7+\frac{7}{9})C$; $R=E_4+\delta E_B+\delta E_C+(23+\frac{1}{3})B+(11+\frac{2}{3})C$. For the $d^6\underline{L}^2$ configuration, only states containing two L_σ holes have been included for simplicity.

(a) Ground state

$\phi_1=|t_{2}^{3}e^{2}\,{}^6A_1\rangle$, $\phi_2=|t_{2}^{3}e^{3}({}^5E)\underline{L}_\sigma\,{}^6A_1\rangle$, $\phi_3=t_{2}^{4}e^{2}({}^5T_2)\underline{L}_\pi\,{}^6A_1\rangle$

$H_{1,1}=K-35B$, $H_{2,2}=L-35B+7C$, $H_{3,3}=L-35B+7C-\delta-\Delta$

$H_{1,2}=\sqrt{2}v_\sigma$, $H_{1,3}=\sqrt{3}v_\pi$

(b) ${}^5E_g$-symmetry final states

$\phi_1=|t_{2}^{3}e^{1}\,{}^5E\rangle$, $\phi_2=|t_{2}^{3}e^{2}({}^6A_1)\underline{L}_\sigma\,{}^5E\rangle$, $\phi_3=|t_{2}^{4}e^{1}({}^4T_1)\underline{L}_\pi\,{}^5E\rangle$

$\phi_4=|t_{2}^{4}e^{1}({}^4T_2)\underline{L}_\pi\,{}^5E\rangle$, $\phi_5=|t_{2}^{3}e^{3}({}^5E)\underline{L}_\sigma^2\,{}^5E\rangle$

$H_{1,1}=P-21B$, $H_{2,2}=Q-35B$, $H_{3,3}=Q-25B+6C-\delta-\Delta$

$H_{4,4}=Q-17B+6C-\delta-\Delta$, $H_{5,5}=R-35B+7C$, $H_{1,2}=v_\sigma$

$H_{1,3}=-\sqrt{3/2}v_\pi$, $H_{1,4}=-\sqrt{3/2}v_\pi$, $H_{2,5}=-1/\sqrt{2}v_\sigma$

(c) ${}^5T_{2g}$-symmetry final states

$\phi_1=|t_{2}^{2}e^{2}\,{}^5T_2\rangle$, $\phi_5=|t_{2}^{2}e^{3}({}^4T_1)\underline{L}_\sigma\,{}^5T_2\rangle$, $\phi_3=|t_{2}^{2}e^{3}({}^4T_2)\underline{L}_\sigma\,{}^5T_2\rangle$

$\phi_4=|t_{2}^{3}e^{2}({}^6A_1)\underline{L}_\pi\,{}^5T_2\rangle$, $\phi_5=|t_{2}^{2}e^{4}({}^3T_1)\underline{L}_\sigma^2\,{}^5T_2\rangle$

$H_{1,1}=P-21B+\Delta$, $H_{2,2}=Q-25B+6C+\Delta$, $H_{3,3}=Q-17B+6C+\Delta$

$H_{4,4}=Q-35B-\delta$, $H_{5,5}=R-29B+12C+\Delta$, $H_{1,2}=v_\sigma$

$H_{1,3}=-v_\sigma$, $H_{1,4}=v_\pi$, $H_{2,5}=-v_\sigma$, $H_{3,5}=v_\sigma$

en from the free-atom values[36] without any renormalization as is usually done in the LF theory. The best fit to the XPS valence-band spectrum was obtained with $\delta E_A=3\pm1$ eV, $\delta E_B=-5\pm0.5$ eV, $\delta E_C=3\pm2$ eV, and $(pd\sigma)=-2(pd\pi)=1.5\pm0.1$ eV as shown in Fig. 9. In order to reproduce the valence-band spectrum, O $2p$ states not hybridizing with Fe $3d$ states have been assumed to have a two-peak structure as discussed in Sec. III A. The relative photoionization cross section of O $2p$ to Fe $3d$ states has been taken 1.8 times larger than the theoretical value for free atoms.[37] Such an enhancement of the O $2p$ cross section has been usually found for transition-metal oxides probably because of modification of the O $2p$ wave functions in a solid-state environment due to, e.g., orbital overlap and charge transfer.[38]

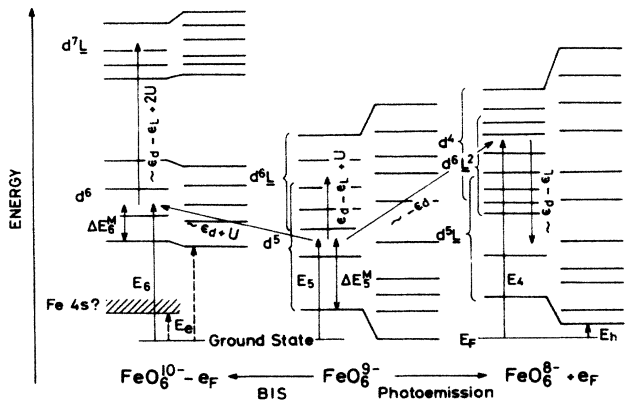

FIG. 8. Schematic energy-level diagram for the FeO_6^{9-} cluster representing the ground state and excitations within the cluster. FeO_6^{8-} and FeO_6^{10-} represent photoemission and BIS final states, respectively. Approximate energy differences between unhybridized configurations are given in terms of ε_d, ε_L, and U. ΔE_n^M is the difference between the lowest multiple component of the d^n configuration and its center of gravity. E_e and E_h are minimum energies required to create an electron and a hole, respectively, from the ground state. e_F denotes an electron at E_F, i.e., photoemission and BIS final-state energies are referenced to the Fermi level, E_F.

Excellent agreement between theory and experiment has been obtained as shown in Fig. 9. The characteristic three-peak structure of the main band as well as the satellite are indeed explained as the Fe $3d$–derived emission, i.e., the multiplet structure of the mixed d^4, $d^5\underline{L}$, and $d^6\underline{L}^2$ configurations. One can also see that the $3d$-derived emission alone (excluding the O $2p$ band contribution) explains the difference between the on- and off-

TABLE III. Reduced transition-matrix elements for $3d$ emission from the FeO_6^{9-} cluster in the high-spin ground state.

$\langle t_{2}^{3}e^{2}\,{}^6A_1||e||t_{2}^{3}e^{1}\,{}^5E\rangle=\sqrt{2}$

$\langle t_{2}^{3}e^{3}({}^5E)\underline{L}_\sigma\,{}^6A_1||e||t_{2}^{3}e^{2}({}^6A_1)\underline{L}_\sigma\,{}^5E\rangle=0$

$\langle t_{2}^{4}e^{2}({}^5T_2)\underline{L}_\pi\,{}^6A_1||e||t_{2}^{4}e^{1}({}^4T_1)\underline{L}_\pi\,{}^5E\rangle=-1$

$\langle t_{2}^{4}e^{2}({}^5T_2)\underline{L}_\pi\,{}^6A_1||e||t_{2}^{4}e^{1}({}^4T_2)\underline{L}_\pi\,{}^5E\rangle=-1$

$\langle t_{2}^{3}e^{2}\,{}^6A_1||t_2||t_{2}^{2}e^{2}\,{}^5T_2\rangle=\sqrt{3}$

$\langle t_{2}^{3}e^{3}({}^5E)\underline{L}_\sigma\,{}^6A_1||t_2||t_{2}^{2}e^{3}({}^4T_1)\underline{L}_\sigma\,{}^5T_2\rangle=\sqrt{3/2}$

$\langle t_{2}^{3}e^{3}({}^5E)\underline{L}_\sigma\,{}^6A_1||t_2||t_{2}^{2}e^{3}({}^4T_2)\underline{L}_\sigma\,{}^5T_2\rangle=-\sqrt{3/2}$

$\langle t_{2}^{4}e^{2}({}^5T_2)\underline{L}_\pi\,{}^6A_1||t_2||t_{2}^{3}e^{2}({}^6A_1)\underline{L}_\pi\,{}^5T_2\rangle=0$

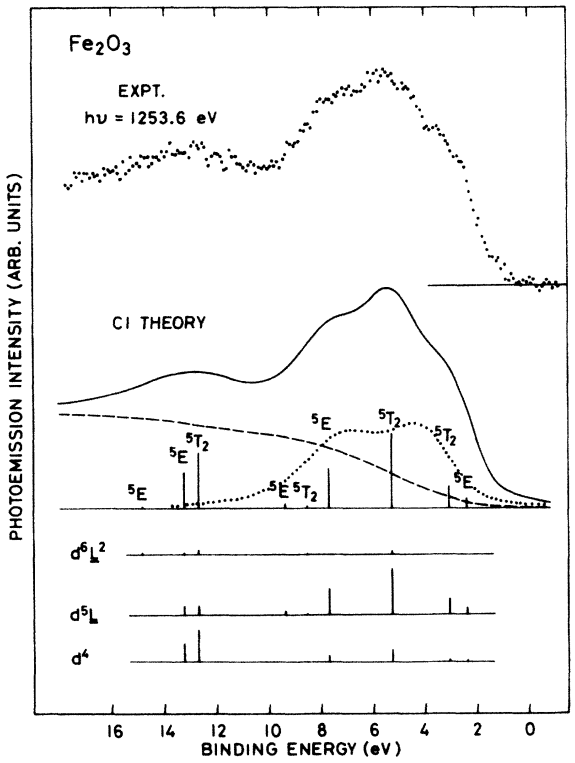

FIG. 9. Theoretical valence-band XPS spectrum of Fe_2O_3 by the FeO_6^{9-} cluster configuration-interaction (CI) calculation compared with experiment. The dotted and dashed curves represent O $2p$ emission and integral background, respectively. The lifetime broadening has been assumed proportional to the binding energy (E_B') relative to the valence-band maximum ($2\gamma = 0.44E_B'$) and a Gaussian full width of 1.5 eV has been employed to represent the combined effects of the instrumental resolution and the d-d hopping (Ref. 16). The bottom panel shows a decomposition into configuration components for each final-state line.

resonance spectra shown in Fig. 3. From the decomposition of the final states into configuration components as shown on the bottom of Fig. 9, the main band, particularly the 2.5-eV feature, is found predominantly $d^5\underline{L}$-like and the satellite largely d^4-like, in agreement with the conjecture made in Sec. III on the experimental basis. It is noted that the 2.5-eV peak consists of two adjacent peaks with ^5E and $^5T_2$ symmetry in striking contrast to the LF theory[13] or the band theory [of MnO (Ref. 14)] according to which the peak has been assigned to a single component, the ^5E_g multiplet term or the e_g band, both originating from e_g electron emission.

V. DISCUSSION

The minimum energy required to create a noninteracting electron-hole pair, $E_e + E_h$ in Fig. 8, is the energy gap measurable by electrical conductivity. E_h corresponds to the top of the O $2p$ band or the lowest energy $d^5\underline{L}$ multiplet, both being of O $2p$ hole character. If E_e is the energy of the lowest multiplet of the d^6 configuration analogous to NiO,[1,3] the system is a p-d charge-transfer insulator according to the classification of Zaanen *et al.*[8] The unoccupied d^6 energy position can be estimated as follows by using U, ε_d, etc., obtained in Sec. IV. The position of the center of gravity of the d^5 configuration, E_5 (Fig. 8), is evaluated 9.4 eV, out of which 7.1 eV is the energy lowering due to the multiplet splitting ΔE_5^M (evaluated using free-atom B and C parameters) and 2.3 eV is the energy lowering due to the hybridization with $d^6\underline{L}$; ε_d has been estimated as -5.8 eV and $U \sim \delta E_A - \delta E_B \simeq (3\pm1) - (-5\pm0.5) \simeq 8\pm2$ eV. Then the position of the lowest d^6 multiplet relative to E_F is given as $\approx E_6 - \Delta E_6^M \simeq E_5 + \varepsilon_d + U - \Delta E_6^M$, where $\Delta E_6^M = 3.7$ eV is the energy lowering due to the multiplet splitting relative to the center of gravity of the d^6 configuration E_6, and is estimated to be 8 ± 2 eV. (A shift due to hybridization with $d^7\underline{L}$ configuration would be small owing to the large d^6-$d^7\underline{L}$ separation, >10 eV.) Actually, this d^6 energy may be reduced by 1—2 eV by further relaxation, but is still estimated to be as large as 6 ± 3 eV above E_F or 8 ± 3 eV above the valence-band maximum. Therefore, an optical absorption edge of 8 ± 3 eV is expected if we consider optical transitions from the valence-band maximum to unoccupied Fe $3d$ states.[39] (Using the same parameter set, an $L \rightarrow d$ charge-transfer excitation energy within the cluster $[E(d^5 \rightarrow d^6\underline{L}) \sim \varepsilon_d - \varepsilon_L + U$ plus hybridization shifts, see Fig. 8] was even estimated as large as ~ 9 eV.) Experimentally, O $2p \rightarrow$ Fe $3d$ charge-transfer optical absorption has been observed at >4.7 eV for dilute Fe^{3+} ions in Al_2O_3 host.[40] This value would be consistent with the O $2p \rightarrow$ Fe $3d$ excitation energy estimated above, if we take into account the different lattice parameters between Al_2O_3:Fe^{3+} and Fe_2O_3 (the latter is larger by $\sim 6\%$) and a possible excitonic effect between the Fe $3d$ electron and the O $2p$ hole.

Thus the present evaluation of the energy gap between the O $2p$ (or $3d^5\underline{L}$) and unoccupied Fe $3d$ (d^6) states is too large to account for the experimental band gap, 2.0—2.7 eV, which was obtained from the electrical conductivity.[31] Presumably the electrical conductivity probes the intrinsic region, since an optical absorption edge of a similar energy, 1.9 eV, has been reported for a Fe_2O_3 film.[41] Thus we propose a possibility that the lowest conduction band is not Fe $3d$ but is of a different origin such as Fe $4s$. The fact that strong optical absorption is absent around ~ 2 eV in Al_2O_3:Fe^{3+} (Ref. 40) would be consistent with this interpretation, because the bottom of the Fe $4s$ band is lowered by several eV for the concentrated Fe ion case in Fe_2O_3 due to a band formation as compared with the impurity Fe^{3+} case. The difference between the conductivity gap, 2.0—2.7 eV, and the optical gap, 1.9 eV, may be attributed to an excitonic effect. Then the electrical conduction takes place via Fe $4s$ electrons and/or O $2p$ (or $d^5\underline{L}$) holes. Such a conduction mechanism is compatible with the transport data.[41] The crossover of the $4s$ band and the unoccupied $3d$ band in going from NiO to Fe oxides is qualitatively consistent with a finding of band calculations[42] that in the series of $3d$ transition-metal

monoxides the metal 4s-derived band is lowered relative to the 3d band in going from heavier to lighter 3d elements. Further, overlap of the metal s band with the 3d band has been suggested to induce insulator-to-metal transitions in 3d transition-metal compounds by Falicov *et al.*[43,44] In particular, for the 3d transition-metal monoxides, they have suggested that the metal 4s band starts to overlap with the occupied part of the 3d band between MnO and VO resulting in the metallic behaviors of VO and TiO.[43]

The multiplet splitting of the d^5 configuration is significantly larger than that of d^6 due to the large exchange interaction in the high-spin d^5 state: ΔE_5^M is larger than ΔE_6^M by as much as 3.4 eV. As can be seen from Fig. 8, the large exchange energy ΔE_5^M leads to a large $d^5\underline{L}$-d^6 band gap and thus, apart from the effect of the metal s band, stabilizes the d^5 local moment against the itinerant d-electron state. This explains why Mn^{2+} compounds such as MnS and MnSe are insulators whereas the neighboring compounds, FeS, FeSe, CrS, and CrSe are metals or narrow-gap semiconductors. Then, one would expect that localized d^4 states in Fe^{4+} and Mn^{3+} compounds are very unstable, since d^5 configuration which is reached by adding an electron to the ground state is subject to a large multiplet splitting pushing down the lowest multiplet component and resulting in a small or vanishing band gap. In fact, $SrFeO_3$ in which Fe is formally tetravalent and MnSb in which Mn is trivalent exhibit metallic behaviors.

The ground-state covalency of Fe_2O_3 is relatively large as can be seen from the large hybridization shift of the ground state, 2.3 eV, within the cluster model. Due to the covalency, the 3d occupancy is shown to increase relative to the purely ionic value of 5 by 0.21 ± 0.05, 80% of which is transferred into the unoccupied e_g orbitals through Fe-O σ bonds. A Mössbauer study of hyperfine fields in $Fe_{2-x}Rh_xO_3$ (Ref. 45) has suggested a transfer of approximately 0.4 electron into the unoccupied, down-spin Fe 3d orbitals in Fe_2O_3, which is twice as large as the value obtained in the present study. The discrepancy would be partly due to the fact that the analyses of the hyperfine fields include charge and spin transfer from the nearest-neighbor Fe atoms (supertransfer hyperfine fields) whereas the present model considers charge transfer only from the nearest neighbor ligands. It should also be noted that the amount of charge transfer estimated in the Mössbauer study depends on assumed values for the Fe 4s-O 2p overlap integral and calculated values for the amplitude of the s-symmetry wave functions at the Fe nucleus.[45] In general, trivalent Fe compounds are supposed to be more covalent than divalent ones, since Fe 3d levels are lowered in the trivalent compounds due to the smaller d-electron occupation. Therefore, the present finding that Fe_2O_3 is a charge-transfer insulator does not necessarily imply that it is also the case for FeO, but our preliminary resonant photoemission results[46] suggest that the lowest binding energy 3d-derived feature in FeO is $d^n\underline{L}$-like as in Fe_2O_3.

The present study has revealed that Fe_2O_3 and Fe^{3+} compounds formed with less electronegative elements than O (and probably FeO and corresponding Fe^{2+} compounds) are in the charge-transfer regime. That is, the present results extend the charge-transfer regime from that initially proposed by Zaanen *et al.*,[8] i.e., Cu, Ni, and Co compounds, to Fe compounds. From the similarity of the photoemission spectra between MnO and Fe_2O_3, MnO might also be considered as a charge-transfer insulator, but a CI theoretical analysis has to still be done to determine the weight of the $d^n\underline{L}$ component in the lowest binding energy photoemission feature. As for Ti and V compounds, Zaanen *et al.* have classified them into the Mott-Hubbard regime. On the other hand, Veal *et al.* have suggested that, in insulating compounds of all 3d transition elements[28] including Ti and V, core holes giving the main (lower binding energy) peaks are screened by d electrons. As 3d electrons and holes in the insulating Ti and V compounds are essentially localized, satellite structures are expected to be similar between the valence-band and core-level photoemission spectra. Therefore, Veal's assignment would suggest that the main valence d bands in the Ti and V compounds correspond to d holes screened by charge transfer into the d orbitals and that these compounds are in the charge-transfer regime rather than in the Mott-Hubbard regime. It is, however, difficult to make a definite conclusion as to which of the two different arguments on the Ti and V compounds is correct, because the two theoretical approaches are not equivalent. Veal *et al.* have treated in the screening process all valence orbitals including metal 4sp in first-principles calculations, but have not considered explicitly charge-transfer processes and the presence of ligand holes in the d-screened final states, which may raise the energies of the d-screened states. Further, it should be noted that screening involving the metal 4sp states may also give rise to distinct satellite features in addition to the d-electron screening as recently pointed out by de Boer *et al.*[47] They have considered a mechanism for the core-level satellites in the insulating 3d transition-metal compounds, where ligand p electrons are excited into unoccupied s orbitals. As the latter mechanism becomes more important with decreasing atomic number of the 3d elements,[47] one has to be careful in analyzing the satellite structures in the light 3d transition-metal compounds.

Finally we would like to comment on the recent suggestion on the temperature dependence of the photoemission spectra of MnO by Ojala and Terakura.[16] They have suggested that the unusually broadwidth of the lowest binding energy d-emission feature of MnO[4] (Fig. 1) compared with that in Mn dichlorides[19] is due to d-d hopping effects. They have proposed a temperature-dependent photoemission experiment in which the d-d hopping, and consequently, the spectral width may be reduced upon antiferromagnetic ordering. According to the present results, however, not only the d-d hopping but also the existence of the two closely spaced $^5T_{2g}$ and ^5E_g multiplet lines can contribute to the width of the lowest binding energy feature. The separation between the two lines and consequently the observed width would vary between materials depending on the d-L transfer integrals, the d and ligand energy levels, the correlation energy U, and the crystal-field splitting. Temperature-dependent photoemission studies would be able to clarify this issue.

VI. CONCLUSION

We have shown that the three-peak structure of the main valence band and the satellite can be explained on the basis of the CI theory: The main and satellite features are assigned to $L \rightarrow d$ screened $d^5\underline{L}$ and unscreened (or poorly screened) d^4 final states, respectively. It is consequently concluded that Fe_2O_3 is a charge-transfer insulator according to the classification of Zaanen *et al.*[6] It is suggested, however, that the lowest unoccupied state may possibly be the bottom of the Fe 4*s* band rather than Fe 3*d* states. The large exchange interaction of the ground-state high-spin d^5 configuration is shown to greatly stabilize the insulating phase with the localized *d* states. This may explain the insulating behaviors of most of Mn^{2+} compounds and the metallic behaviors of some Fe^{4+} and Mn^{3+} compounds, as localized d^4 configurations tend to be unstable and to become itinerant. An extension of the present work to lighter 3*d* elements would reveal changes of the d^{n-1} versus the $d^n\underline{L}$ final states in the photoemission spectra with decreasing atomic number in relation to charge-transfer versus Mott-Hubbard behaviors in the light 3*d* transition-metal compounds. Effects of the metal 4*s* band on metal-insulator transitions are also important questions to be addressed. Fe compounds formed with more electropositive elements such as Fe sulphides will also reveal interesting changes in the electronic structure concerning the same problems.

ACKNOWLEDGMENTS

The authors would like to thank Miss T. Mori, Dr. K. Soda, and the staff of Synchrotron Radiation Laboratory for technical support. Thanks are also due to Mr. M. Sekita for the data aquisition system of the XPS spectrometer and to Dr. F. Minami for help with the cluster calculation. They are much obliged to Professor S.-J. Oh for fruitful discussions.

[1]A. Fujimori, F. Minami, and S. Sugano, Phys. Rev. B **29**, 5225 (1984); A. Fujimori and F. Minami, *ibid.* **30**, 957 (1984).

[2]S. Hüfner, F. Hulliger, J. Osterwalder, and T. Riesterer, Solid State Commun. **50**, 83 (1984).

[3]G. A. Sawatzky and J. W. Allen, Phys. Rev. Lett. **53**, 2339 (1984); S. Hüfner, J. Osterwalder, T. Riesterer, and F. Hulliger, Solid State Commun. **52**, 793 (1984).

[4]D. E. Eastman and J. L. Freeouf, Phys. Rev. Lett. **34**, 395 (1975).

[5]N. F. Mott, Proc. Phys. Soc. London, Sect. A **62**, 416 (1949); J. Hubbard, Proc. R. Soc. London Ser. A **277**, 237 (1964); **281**, 401 (1964); for review, see B. H. Brandow, Adv. Phys. **26**, 651 (1977).

[6]S. Hüfner, T. Riesterer, and F. Hulliger, Solid State Commun. **54**, 689 (1985).

[7]J. Zaanen, G. A. Sawatzky, and J. W. Allen, J. Magn. Magn. Mater. **54-57**, 607 (1986).

[8]J. Zaanen, G. A. Sawatzky, and J. W. Allen, Phys. Rev. Lett. **55**, 418 (1985).

[9]K. Shiratori, S. Suga, M. Taniguchi, K. Soda, S. Kimura, and A. Yanase, J. Phys. Soc. Jpn. **55**, 690 (1986).

[10]D. Ihle and B. Lorenz, Philos. Mag. B **42**, 337 (1980); B. K. Chakraverty, *ibid.* 373 (1980).

[11]For example, G. C. Allen, P. M. Tucker, and R. K. Wild, Philos. Mag. B **46**, 411 (1982); Y. Sakisaka, T. Miyano, and M. Onchi, Phys. Rev. B **30**, 6849 (1984); M. G. Ramsey and G. J. Russell, Phys. Rev. B **30**, 6960 (1984).

[12]S. Sugano, Y. Tanabe, and H. Kamimura, *Multiplets of Transition-Metal Ions in Crystals* (Academic, New York, 1970).

[13]N. Beatham, A. F. Orchard, and G. Thornton, J. Phys. Chem. Solids **42**, 1051 (1981).

[14]T. Oguchi, K. Terakura, and A. R. Williams, Phys. Rev. B **28**, 6443 (1983).

[15]K. Terakura, A. R. Williams, T. Oguchi, and J. Kübler, Phys. Rev. Lett. **52**, 1830 (1984).

[16]E. J. Ojala and K. Terakura, Phys. Rev. B **33**, 2733 (1986).

[17]C. R. Brundle, T. J. Chuan, and K. Wandelt, Surf. Sci. **68**, 459 (1977).

[18]T. Ishii, S. Kono, S. Suzuki, I. Nagakura, T. Sagawa, R. Kato, M. Watanabe, and S. Sato, Phys. Rev. B **12**, 4320 (1975).

[19]A. Kakizaki, K. Sugeno, T. Ishii, H. Sugawara, I. Nagakura, and S. Shin, Phys. Rev. B **28**, 1026 (1983); A. Kakizaki, T. Miya, K. Naito, I. Fukui, H. Sugawara, I. Nagakura, and T. Ishii, J. Phys. Soc. Jpn. **44**, 3638 (1985).

[20]J. J. Yeh and I. Lindau, At. Data Nucl. Data Tables **32**, 1 (1985). In this reference as well as in Ref. 37, the O 2*p* cross section for $h\nu \sim 1200-1500$ eV has been calculated to be too small compared with experiments on metal oxides by a factor of 2—3 as is pointed out in Ref. 38. From the present experimental data, it seems that a similar discrepancy exists down to $h\nu \sim 20$ eV.

[21]W. J. Gignac, R. S. Williams, and S. P. Kowalczyk, Phys. Rev. B **32**, 1237 (1985).

[22]For review, see L. C. Davis, J. Appl. Phys. **59**, R25 (1986).

[23]L. C. Davis, Phys. Rev. B **25**, 2912 (1982); G. van der Laan, Solid State Commun. **42**, 165 (1982).

[24]R. Bruhn, E. Schmidt, H. Schöder, and B. Sonntag, Phys. Lett. **90A**, 41 (1982).

[25]S. Shin, S. Suga, M. Taniguchi, H. Kanzaki, S. Shibuya, and T. Yamaguchi, J. Phys. Soc. Jpn. **51**, 906 (1982).

[26]G. van der Laan, J. Zaanen, G. A. Sawatzky, R. Karnatak, and J.-M. Esteva, Phys. Rev. B **33**, 4253 (1986).

[27]S. P. Kowalczyk, L. Ley, F. R. McFeely, and D. A. Shirley, Phys. Rev. B **11**, 1721 (1975).

[28]See, e.g., T. A. Carlson, J. C. Carver, L. K. Saethre, F. Garcia Santibanez, and G. A. Vernon, J. Electron Spectrosc. Relat. Phenom. **5**, 247 (1974).

[29]B. W. Veal and A. P. Paulikas, Phys. Rev. Lett. **51**, 1995 (1983); Phys. Rev. B **31**, 5399 (1985); B. W. Veal, D. E. Ellis, and D. J. Lam, Phys. Rev. B **32**, 5391 (1985).

[30]The band structure of the corundum-structure V_2O_3 has been calculated by J. Ashkenazi and M. Weger [J. Phys. (Paris) Colloq. **37**, C4-189 (1976)] and a total *d*-band width of ~ 9 eV has been obtained. In Fe_2O_3 the bandwidth would be reduced from this value due to the smaller radial extent of the Fe 3*d* orbitals and also by the antiferromagnetic ordering but would still be of the order of ~ 1 eV (see Ref. 14).

[31]S. Mochizuki, Phys. Status Solidi A **41**, 591 (1977); K.-H. Kim, S.-H. Lee, and J.-S. Choi, J. Phys. Chem. Solids **46**, 331

(1985).

[32]Y. Jugnet and T. M. Duc, J. Phys. Chem. Solids **40**, 29 (1979).

[33]In the present paper unlike Ref. 1, the atomic-orbital bases have been assumed to be orthogonal between Fe and O sites: $S_\sigma = S_\pi = 0$. Further, O $2s$ states have not been included. These simplifications have reduced the computational effort compared with Ref. 1 but there is no important change in the physics and the calculated results. Recently a calculation using the same procedure has been performed for another high-spin d^5 system $Cd_xMn_{1-x}Te$, where a Mn atom is tetrahedrally coordinated by Te atoms [L. Ley, M. Taniguchi, J. Ghijsen, R. L. Johnson, and A. Fujimori, submitted to Phys. Rev. B.

[34]The center of gravity of the d^n configuration includes the average exchange energy of that configuration and therefore the energy difference between the centers of gravity of different configurations is a function not only of U but also of B and C. However, because the average exchange energy varies approximately linearly with the d-electron number, the same U value is obtained from $U \sim \delta E_A - \delta E_B$ either by including or excluding the average exchange energy.

[35]$\Delta(^{2S+1}\Gamma)$ includes also a crystal-field splitting due to the electrostatic field induced by the ligand atoms, denoted by $\Delta \equiv \varepsilon(e_g) - \varepsilon(t_{2g})$ in Table II. Δ is negative and an order of magnitude smaller than the crystal-field splitting due to the d-L hybridization (Ref. 42). In the present calculation, Δ is taken as -0.4 eV so as to give the best resemblance of the calculated spectrum to the experiment.

[36]Y. Tanabe and S. Sugano, J. Phys. Soc. Jpn. **9**, 767 (1954). As B and C parameters for the Fe^{4+} ion (d^4 configuration) are not found in this reference, they have been extrapolated from those for the $Fe^{2+}(d^6)$ and $Fe^{3+}(d^5)$ ions.

[37]J. H. Scofield, J. Electron Spectrosc. Relat. Phenom. **8**, 129 (1976).

[38]G. A. Sawatzky and D. Post, Phys. Rev. B **20**, 1546 (1977).

[39]The top of the O $2p$ band and the lowest binding energy $d^5\underline{L}$ final state have nearly the same energies within an accuracy of $\lesssim 1$ eV as can be seen from Fig. 9.

[40]H. H. Tippins, Phys. Rev. B **1**, 126 (1970).

[41]F. J. Morin, Phys. Rev. **93**, 1195 (1954).

[42]L. F. Mattheiss, Phys. Rev. B **5**, 290 (1972).

[43]R. Ramirez, L. M. Falicov, and J. C. Kimball, Phys. Rev. B **2**, 3383 (1970).

[44]B. Koiller and L. M. Falicov, J. Phys. C **7**, 299 (1974).

[45]J. M. D. Coey and G. A. Sawatzky, J. Phys. C **4**, 2386 (1971).

[46]A. Fujimori, N. Kimizuka, M. Taniguchi, and S. Suga (unpublished).

[47]D. K. G. De Boer, C. Hass, and G. A. Sawatzky, Phys. Rev. B **29**, 4401 (1984).